 doi:10.20944/preprints202205.0050.v1

Article

Improved unsupervised learning method for material properties identification based on mode separation of ultrasonic guided waves

Mikhail V. Golub [1], Olga V. Doroshenko[1], Mikhail A. Arsenov[1], Artem A. Eremin* [1], Yan Gu[2], Ilya A. Bareiko[1]

[1] Institute for Mathematics, Mechanics and Informatics, Kuban State University, Krasnodar 350040, Russian Federation; m_golub@inbox.ru (M.V.G.); oldorosh@mail.ru (O.V.D.); mihail2212@mail.ru (M.A.A); ilyabareiko@yandex.ru (I.A.B.); eremin_a_87@mail.ru(A.A.E.);
[2] School of Mathematics and Statistics, Qingdao University, Qingdao 266071, PR China; guyan1913@163.com (Y.G.)
* Correspondence: m_golub@inbox.ru;

Abstract: Numerical methods, including machine learning methods, are now actively used in the applications related to guided wave propagation. The method proposed in this study for material properties characterization is based on the algorithm of the clustering of multivariate data series obtained as a result of the application of the matrix pencil method to the experimental data. In the proposed technique, multi-objective optimization is employed to improve the accuracy of particular parameter identification. At the first stage, the computationally efficient method based on the calculation of the Fourier transform of Green's matrix is employed iteratively and the obtained solution is used for the filter construction with decreasing bandwidth, which allows us to obtain nearly noise-free classified data (with mode separation). The filter provides data separation between all guided waves in a natural way, which is needed at the second stage, where the slower method based on the minimization of the slowness residuals is applied to the data. The method might be applied for material properties identification in plates with thin coatings/interlayers, multi-layered anisotropic laminates etc.

Keywords: laminate; material properties; identification; guided waves; mode separation;

1. Introduction

Noninvasive characterization of material mechanical properties is vital for condition monitoring to control the quality of samples and to identify possible damage or structural degradation during its service period [1]. Vibration-based techniques have proven their efficiency for the evaluation of elastic properties of small-scale samples [2]. However, due to the "global" nature of these approaches, their applicability for the characterization of certain structural parts, especially in large-scale engineering assemblies, might be restrained. Meanwhile, methods relying on ultrasonic guided waves (UGWs) provide an appropriate compromise between "global" and "local" structural evaluation and thus might serve as a suitable basis for corresponding non-destructive testing and structural health monitoring applications [3–8]. UGWs are multi-modal waves and using them for material properties identification often requires laborious signal processing. On the other hand, the benefit of the multi-modal nature is the availability of information on the wave characteristics in a wide frequency range, which improves the identification procedure. For instance, Cui and Lanza di Scalea [9] applied the advanced simulated annealing optimization algorithm to match pseudo-experimental phase velocity curves for fundamental modes (S0, A0, SH0) to computed velocity curves with varying constants in anisotropic laminate. It was shown in [10], where the fuzzy-based inversion technique was applied for the identification problem, that the inclusion of all UGWs better consolidates the identified uncertainties of the material properties compared to single-mode analysis in a broader frequency range. For the identification algorithms, the UGWs separation is necessary, which is still challenging, since the dispersion effect leads to modal amplitudes of different levels and overlapping of

Citation: Golub, M.V.; Doroshenko, O.V.; Arsenov, M.A.; Eremin, A.A.; Gu, Y.; Bareiko, I.A. Improved unsupervised learning method for material properties identification. *Preprints* **2022**, *1*, 0. https://doi.org/

Received:
Accepted:
Published:

 doi:10.20944/preprints202205.0050.v1

the wave packages in the time-frequency domains. A significant number of researchers use the frequency-wavenumber representation, where the energy distributions of individual modes are naturally separated from each other. There are examples of the successful application of the matrix pencil method (MPM) and estimation of signal parameters via rotational invariance techniques (ESPRIT) based on the eigenvalue decomposition, such as singular value decomposition (SVD) [11–13]. Unfortunately, the number of modes is often not easily determined from thresholds using only eigenvalue intensities or singular values, and Okumura *et al.* [14] proposed an algorithm applying information-theoretic criteria efficient for SVD and ESPRIT methods. In [15], to obtain a time-frequency representation, an inverse synchronized wavelet transform was used, which makes it possible to automatically select individual modes after image processing. A time-frequency method of multi-modal dispatcher dispersion was also proposed for mode separation by Xu *et al.* [16]. However, the problem of automatic UGW separation is not fully solved at the moment.

Machine learning methods are now actively used in UGW propagation problems like the mode separation related to unsupervised and self-supervised methods. Non-negative matrix factorization was employed for mode separation with subsequent classic clustering algorithm (DBSCAN) [17]. Convolutional neural network (CNN) were applied for automatic selection of dispersion curves for the fundamental and higher modes of the 2D seismic profile [18], while a deep neural network (DNN) was trained to reconstruct plane wave ultrasound images from RF channel [19]. The clustering of series of data points algorithm based on the feature extraction from multi-dimensional data was used for estimating complex frequencies and amplitudes of signals [13]. For machine learning algorithms related to the identification of waveguide parameters, supervised learning methods have been also used recently, for instance, in [8,20–22], and the learning took place on synthetic data.

The principle of the method discussed in the current paper is based on the algorithm of the clustering of multivariate data series obtained as a result of the application of the MPM to the experimental data. In the proposed technique, multi-objective optimization is employed, which is usually used to improve the accuracy of particular parameter identification [23]. At the first stage, the computationally efficient method based on the calculation of the Fourier transform of Green's matrix (GMM) is employed (see [24] and references therein) iteratively, and the obtained solution is used for the filter construction with decreasing bandwidth, which allows us to obtain nearly noise-free classified data (with mode separation). The filter provides data separation between all UGWs in a natural way, which is needed at the second stage, where the slower method based on the minimization of the slowness residuals (SRM) is applied to the data. The second step is important since the SRM is more accurate than the GMM. On the other hand, the first step is indispensable to providing mode separation needed for the SRM.

2. Data extraction and initialization

Various scanning techniques (laser Doppler vibrometry, phased arrays, air-coupled transducers) can be applied to obtaining data, which is necessary for data extraction in the first step. Let us consider an elastic plate, where the Cartesian coordinates are introduced so that the scan line goes along the Ox-axis, and the source exciting GWs is situated at the origin of coordinates. Further on, it is assumed that the laser Doppler vibrometry is employed as a method for data acquisition at the surface $z = 0$ of the specimen (out-of-plane velocities or displacements) since it provides minimal distortion to the measured wavesignals [25].

It should be noted here that the method of data acquisition at the surface $z = 0$ of the specimen (out-of-plane velocities or displacements) is not important for the proposed method (see Figure 1). Let us assume that velocities or displacements denoted for simplicity as $v(x, 0, 0, t)$ are measured at points $(x_i, 0, 0)$ at the moments of time t_k, and $v(x_i, t_k) = v_{ik}$. According to the MPM, the Fourier transform is applied to $v(x_i, t_k)$ with respect to time-

Preprints (www.preprints.org) | NOT PEER-REVIEWED | Posted: 5 May 2022 doi:10.20944/preprints202205.0050.v1

variable for a certain set of frequencies $f_n, n = \overline{1, N_\mathrm{f}}$, which gives $V(x_i, f_n) = V_i^n$. The MPM is applied to determine the relation between the wavenumber k and the frequency f.

Thus, for a certain frequency f_n and a given set of scan points x_i, the following approximation is to be constructed:

$$V_i^n \approx \sum_{m=1}^{M} A_m^n z_{mn}^{i-1} = \sum_{m=1}^{M} A_m^n \mathrm{e}^{\mathrm{i}\, k_{mn}\, \Delta x\, (i-1)}, \tag{1}$$

where Δx is the spatial step in the line scan, A_m^n are amplitudes related to poles z_{mn}, which corresponds to guided waves with wavenumbers k_{mn} propagating at frequency f_n.

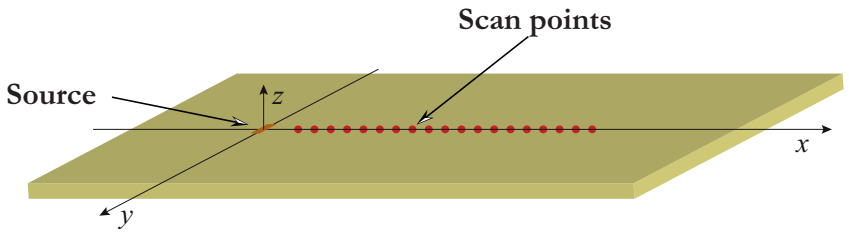

Figure 1. Geometry of the problem considered.

Therefore, for n-th frequency f_n from a certain set of frequencies, matrix pencil of two Hankel matrices $\mathbf{X}$ and $\mathbf{Y}$ are composed from the values U_i^n. Employing the singular value decomposition, for $\mathbf{X} = \mathbf{U} \cdot \mathbf{\Lambda} \cdot \mathbf{V}$, where $\mathbf{U}$ and $\mathbf{V}$ are unitary matrices and $\widetilde{\mathbf{\Lambda}} = \mathrm{diag}(\lambda_1, \ldots)$ is rectangular diagonal matrix. Then, the eigenvalues of matrix pencil $(\mathbf{X}, \mathbf{Y})$ are determined using reduced singular value decomposition of matrix $\mathbf{X} = \widetilde{\mathbf{U}} \cdot \widetilde{\mathbf{\Lambda}} \cdot \widetilde{\mathbf{V}}$, which is obtained via the reduction of the first largest M singular values in $\mathbf{\Lambda}$, i.e. $\widetilde{\mathbf{\Lambda}} = \mathrm{diag}(\lambda_1, \ldots, \lambda_M)$ and $\widetilde{\mathbf{U}}$ and $\widetilde{\mathbf{V}}$ are corresponding unitary matrices. Therefore, the problem can be reduced to the eigenvalue problem for

$$\widetilde{\mathbf{U}}^* \cdot \mathbf{X} \cdot \widetilde{\mathbf{V}}^* - z\widetilde{\mathbf{\Lambda}}$$

with respect to z-values, which gives values of k_{nj}. It should be mentioned that the number of poles M can be chosen specifically for each frequency.

An example of the MPM application to determine dispersion properties of an aluminium plate of 2 mm thickness is depicted in Figure 2, where slownesses $s_{nm} = k_{nm}/f_n$ have been calculated for 200 frequencies $f_n \in [0.5, 2.4]$ MHz.

Thus, the MPM described in this section is applied at the first step to extract slowness-frequency pairs $\breve{\boldsymbol{g}} = \{(\breve{s}_{nm}, f_n), m = \overline{1, M}\}$ from the raw experimental signals (the parameter M of the MPM should be chosen with an assurance that it is larger than the number of propagating guided waves). Unfortunately, the data is usually noisy, and certain noise removal is needed.

The amplitudes A_m^n obtained after decomposition (1) are normalized for each frequency:

$$A_m^n := A_m^n / \max_m(A_m^n), \quad n = \overline{1, N_\mathrm{f}}.$$

Further, the points with amplitudes $A_m^n < 0.1$ are removed from the dataset to clean up the noise. It should be noted that the increase of this threshold of 0.1 leads not only to the removal of the noise but also deletes the points belonging to the dispersion curves themselves (it could lead to a full disappearance of some modes which have not been intensively excited in the experiment). Such a noise removal gives the set of slowness-frequency pairs

$$\breve{\boldsymbol{g}} := \{(s_{nm}, f_n), m \in \mathcal{B}_n, n = \overline{1, N_\mathrm{f}}\},$$

where the fact that the number of pairs varies from frequency to frequency is taken into account via the introduction of sets $\mathcal{B}_n = \{m | \breve{A}_{nm} > 0.1\}$. Here N_f is the total number of frequencies f_n in the set $\boldsymbol{g}$.

Preprints (www.preprints.org) | NOT PEER-REVIEWED | Posted: 5 May 2022 doi:10.20944/preprints202205.0050.v1

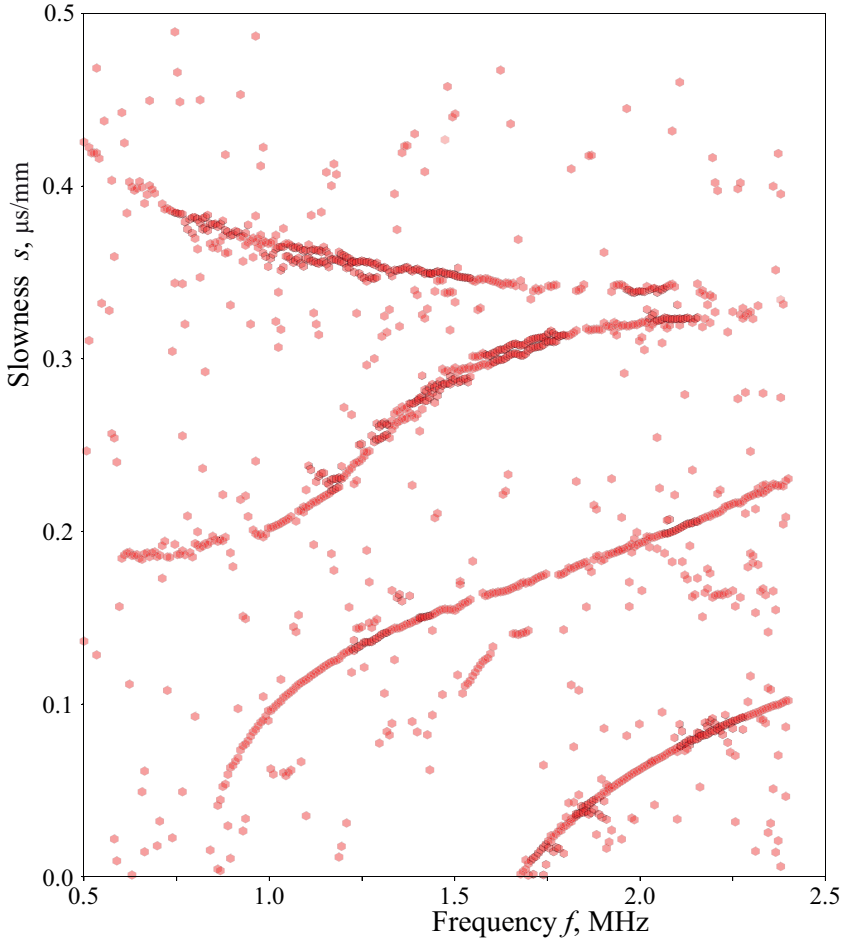

Figure 2. The slownesses calculated for 2 mm thickness aluminium plate using the MPM at $M = 6$.

3. Objective functions

3.1. Method based on the calculation of the Fourier transform of Green's matrix

At the first stage of the proposed identification procedure the GMM avoiding time-consuming root search procedures is applied. In the GMM, the minimization of objective function $G(\boldsymbol{\theta}, \boldsymbol{g})$ is performed so that the estimate is determined as follows:

$$\hat{\boldsymbol{\theta}} = \arg\min_{\boldsymbol{\theta}\in\Theta} G(\boldsymbol{\theta}, \breve{\boldsymbol{g}}).$$

Here, $\boldsymbol{\theta}$ is the vector of the parameters of the model and Θ denotes the bounds of the model parameters. The objective function $G(\boldsymbol{\theta}, \breve{\boldsymbol{g}})$ for the GMM is defined via the replacement of the frequency f and slowness s into the inversion of the Fourier transform of Green's matrix component $K_{33}^{-1}(f, s, 0, \boldsymbol{\theta})$:

$$G(\boldsymbol{\theta}, \boldsymbol{g}) = \frac{1}{N}\sum_{n=1}^{N_\mathrm{f}}\sum_{m\in\mathcal{B}_n} \min\Big(|K_{33}^{-1}(f_n, \breve{s}_{nm}, 0, \boldsymbol{\theta})|, 1\Big), \tag{2}$$

$$N = \sum_{n=1}^{N_\mathrm{f}} |\mathcal{B}_n|.$$

An upper limit is introduced to avoid large values of objective function (2), which improves the effectiveness of the inversion procedure, since extremely large values could strongly influence the objective function [24]. For the examples considered in this study, the Fourier

Preprints (www.preprints.org) | NOT PEER-REVIEWED | Posted: 5 May 2022 doi:10.20944/preprints202205.0050.v1

transform of Green's matrix of an elastic homogeneous layer is used, but the proposed identification approach is also applicable for other kinds of waveguides.

Let us briefly describe the scheme of Green's matrix composition in the case of a homogeneous stress-free elastic layer $V = \{|x| < \infty, -H \le z \le 0\}$ of thickness H with the mass density ρ, Young's modulus E and Poisson's ratio ν (see Figure 1). At least one parameter must be already determined for identification, otherwise, the solution is not unique. For the steady-state motion with the angular frequency $\omega = 2\pi f$, the displacement vector $\boldsymbol{u}$ in an elastic homogeneous isotropic media satisfies the governing equations:

$$\frac{1-\nu}{1-2\nu}\nabla\cdot\nabla\boldsymbol{u} - \frac{1}{2}\nabla\times(\nabla\times\boldsymbol{u}) + \frac{(1+\nu)\rho}{E}\omega^2\boldsymbol{u} = \boldsymbol{0}. \tag{3}$$

The stress-free boundary conditions (the Hooke's law relates the components of the displacement vector $\boldsymbol{u}$ and the stress tensor σ_{ik}) are assumed at the surfaces of the waveguide

$$\sigma_{i2}(x,0) = \sigma_{i2}(x,-H) = 0, \qquad \forall x. \tag{4}$$

The application of the Fourier transform to governing equations (3) with respect to x_1 and boundary conditions (4) leads to the system of ordinary differential equations, where the unit vector is given in the right-hand side. The solution of the obtained system allows calculating the Fourier transform of Green's matrix (see [26] for more details).

3.2. Method based on the slowness residuals

In the second approach, the minimization of the residuals between measured slownesses $\check{s}_{nm}$ and theoretical slownesses $s_{nm}(\boldsymbol{\theta}, f_n)$ calculated employing the mathematical model (e.g. described in Section 3.1) with the parameter $\boldsymbol{\theta}$ at given frequency f_n, see [24] for more details. To calculate the objective function

$$S(\boldsymbol{\theta}, \boldsymbol{g}) = \frac{1}{N}\sum_{n=1}^{N_\mathrm{f}}\sum_{m\in\mathcal{B}_n}|\check{s}_{nm} - s_{nm}(\boldsymbol{\theta}, f_n)|, \tag{5}$$

an accurate procedure for the mode separation is needed since the distance between theoretical and experimental slownesses corresponding to the same guided wave should be compared. Another disadvantage of the use of this objective function is related to the numerical search of the roots of the dispersion equation, which is obtained via the application of the Fourier transform with respect to x_1 to governing equations (3) and boundary conditions (4) for each frequency f_n. The latter makes solution of the optimization problem

$$\hat{\boldsymbol{\theta}} = \arg\min_{\boldsymbol{\theta}\in\Theta} S(\boldsymbol{\theta}, \check{\boldsymbol{g}})$$

computationally expensive.

4. Multi-stage algorithm for material properties characterization

The method proposed here is a combination of two approaches for material properties identification, which convergence and accuracy was analysed by Golub *et al.* [24]. It was shown in [24] that the method based on the slowness residuals (SRM) is time-consuming since it needs multiple calls for mode separation and search-root procedures. The computational time for the second method based on the calculation of the Fourier transform of Green's matrix (GMM) is hundred times smaller than for the SRM, but the accuracy of the SRM is better (the GMM usually overestimates parameter values). All the stages of the proposed algorithm for waveguide properties identification are briefly described in the flowchart shown in Figure 3, whereas detailed description of the stages can be found in Sections 2–3.

Step 1. In the first step, extraction of the information on dispersion characteristics of an inspected waveguide is performed. To this end, the MPM is applied to the experimental

Preprints (www.preprints.org) | NOT PEER-REVIEWED | Posted: 5 May 2022 doi:10.20944/preprints202205.0050.v1

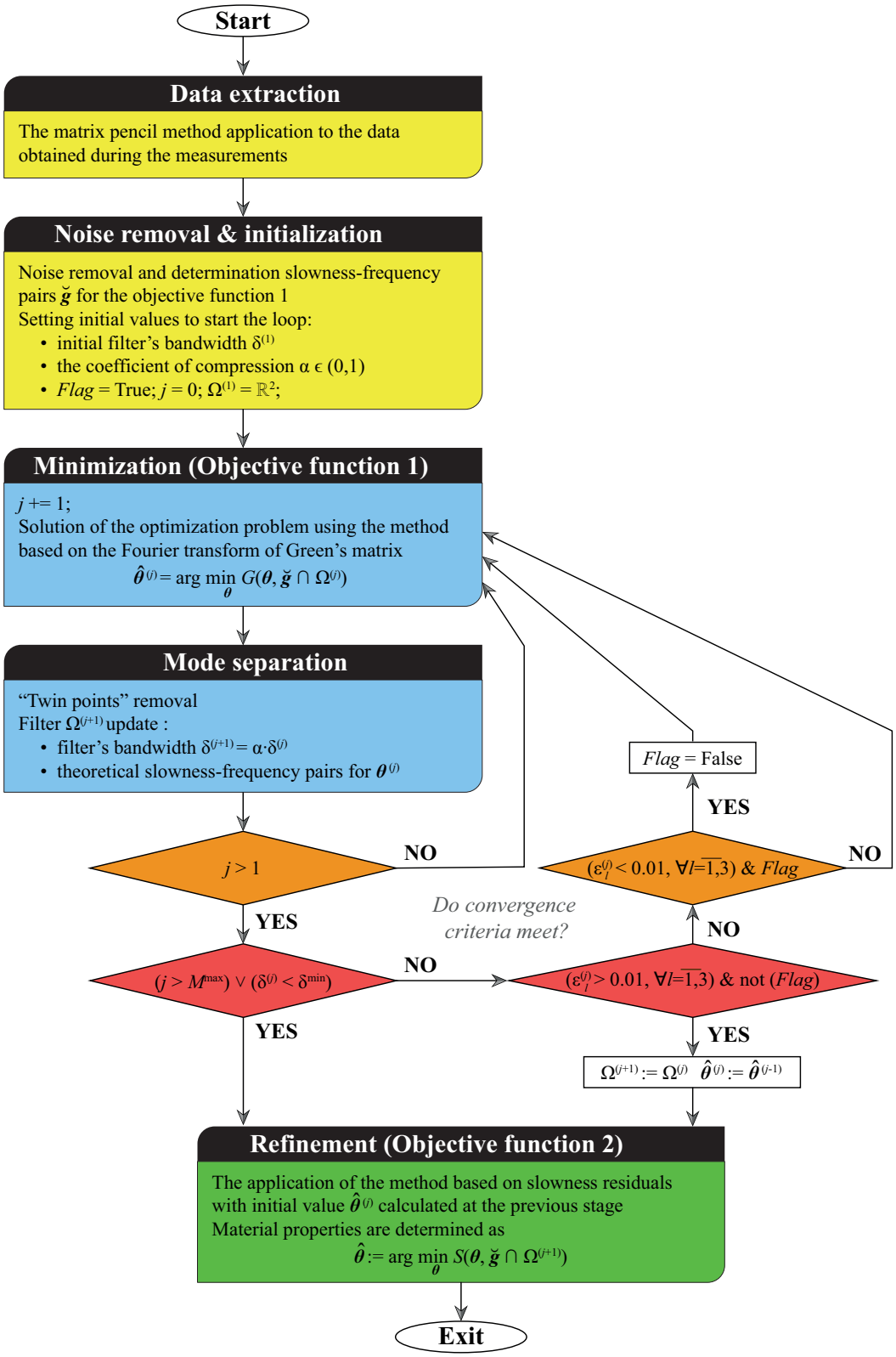

Figure 3. Flowchart of the proposed multi-stage algorithm.

signal and some noise is removed as described in Section 2. Before starting the loop at the next step, the bandwidth of filter $\delta^{(1)}$, the coefficient of filter bandwidth compression $\alpha \in (0,1)$ and bounds Θ, where the solution is allowed, are chosen. Also, initial values

Preprints (www.preprints.org) | NOT PEER-REVIEWED | Posted: 5 May 2022 doi:10.20944/preprints202205.0050.v1

$\Omega^{(1)} = \mathbb{R}^2$, $\breve{\boldsymbol{g}}^{(1)} = \breve{\boldsymbol{g}}$ and $j = 0$ necessary for the first stage of the identification procedure are determined at this step.

Step 2. An iterative procedure is repeated at the second step until the convergence criteria described further are met. According to the GMM, the solution of the optimization problem

$$\hat{\boldsymbol{\theta}}^{(j)} = \arg\min_{\boldsymbol{\theta}\in\Theta} G(\boldsymbol{\theta}, \breve{\boldsymbol{g}}^{(j)}) \tag{6}$$

is obtained at j-th iteration using the Broyden-Fletcher-Goldfarb-Shanno (BFGS) method. Here $\Omega^{(j)}$ describes the action of the filter

$$\breve{\boldsymbol{g}}^{(j+1)} = \breve{\boldsymbol{g}} \cap \Omega^{(j+1)}$$

extracting from $\breve{\boldsymbol{g}}$ only the pairs laying in $\delta^{(j)}$-vicinity of the theoretical slowness curves, i.e.

$$\Omega^{(j+1)}) = \left\{(s,f) | s(\hat{\boldsymbol{\theta}}^{(j)}, f) - \delta^{(j)} \le s \le s(\hat{\boldsymbol{\theta}}^{(j)}, f) + \delta^{(j)}\right\}.$$

The bandwidth of the filter decreases at each iteration:

$$\delta^{(j+1)} = \alpha \cdot \delta^{(j)}.$$

The process is repeated at least two times. At the first iteration no criteria are checked, then relative error

$$\varepsilon_l^{(j)} = \frac{\hat{\theta}_l^{(j)} - \hat{\theta}_l^{(j-1)}}{\hat{\theta}_l^{(j)}}$$

is considered to break the loop. Two-step criteria is proposed, and logical variable *Flag* (initial value is *Flag*=True) is used in the flowchart to explain the algorithm. Starting from the second loop, the condition $\varepsilon_l^{(j)} < 0.01$ is checked, and as soon it is satisfied logical variable changes it value (*Flag*=False). This condition is demanded to assure that the search becomes stable. The second condition is checked only if the first one is satisfied. The condition examines whether the search procedure is still stable and if the condition $\varepsilon_l^{(j)} < 0.01$ is not satisfied anymore the loop is finished at j-th iteration setting $\hat{\theta}_l^{(j)} := \hat{\theta}_l^{(j-1)}$ and $\Omega^{(j+1)}) := \Omega^{(j)})$. Of course, the criteria related to the largest number of iterations ($j > M^{\max}$) and the minimum bandwidth of the filter ($\delta^{(j)} < \delta^{\min}$) are also checked before continuing each loop for $j > 2$.

Step 3. The converged solution $\hat{\theta}_l^{(j)}$ obtained at *Step* 2 applying the GMM in (6) is subsequently refined at the last step using the SRM method:

$$\hat{\boldsymbol{\theta}} = \arg\min_{\boldsymbol{\theta}\in\Theta} S(\boldsymbol{\theta}, \breve{\boldsymbol{g}}^{(j)}). \tag{7}$$

Since filter $\Omega^{(j+1)})$ separates modes, numbers of guided waves are easily distinguished in the SRM. To have better estimates, the optimization can be run several times using $\hat{\boldsymbol{\theta}}^{(j)}$ with a random additive less than 1% as an initial value for the minimization procedure. In this case, mean or median can be chosen to obtain a statistically accurate estimate for the material properties.

5. Examples of material properties identification using experimental data

The proposed algorithm has been verified and tested using experimental data measured for three different plates. Their thickness H and elastic properties, i.e. Young's modulus and Poisson's ratio, are unknown while density ρ is assumed being known in advance. Ultrasonic GWs have been excited in rectangular plates made of aluminium ($\rho = 2660$ kg/m^3 and $H = 2$ mm), duralumin ($\rho = 2721$ kg/m^3 and $H = 1.9$ mm) and steel ($\rho = 7843$ kg/m^3 and $H = 1.975$ mm) by a circular piezoelectric actuator of 5 mm radius and 0.5 mm thickness manufactured from PZT PIC 151 (PI Ceramic GmbH, Germany).

Preprints (www.preprints.org) | NOT PEER-REVIEWED | Posted: 5 May 2022 doi:10.20944/preprints202205.0050.v1

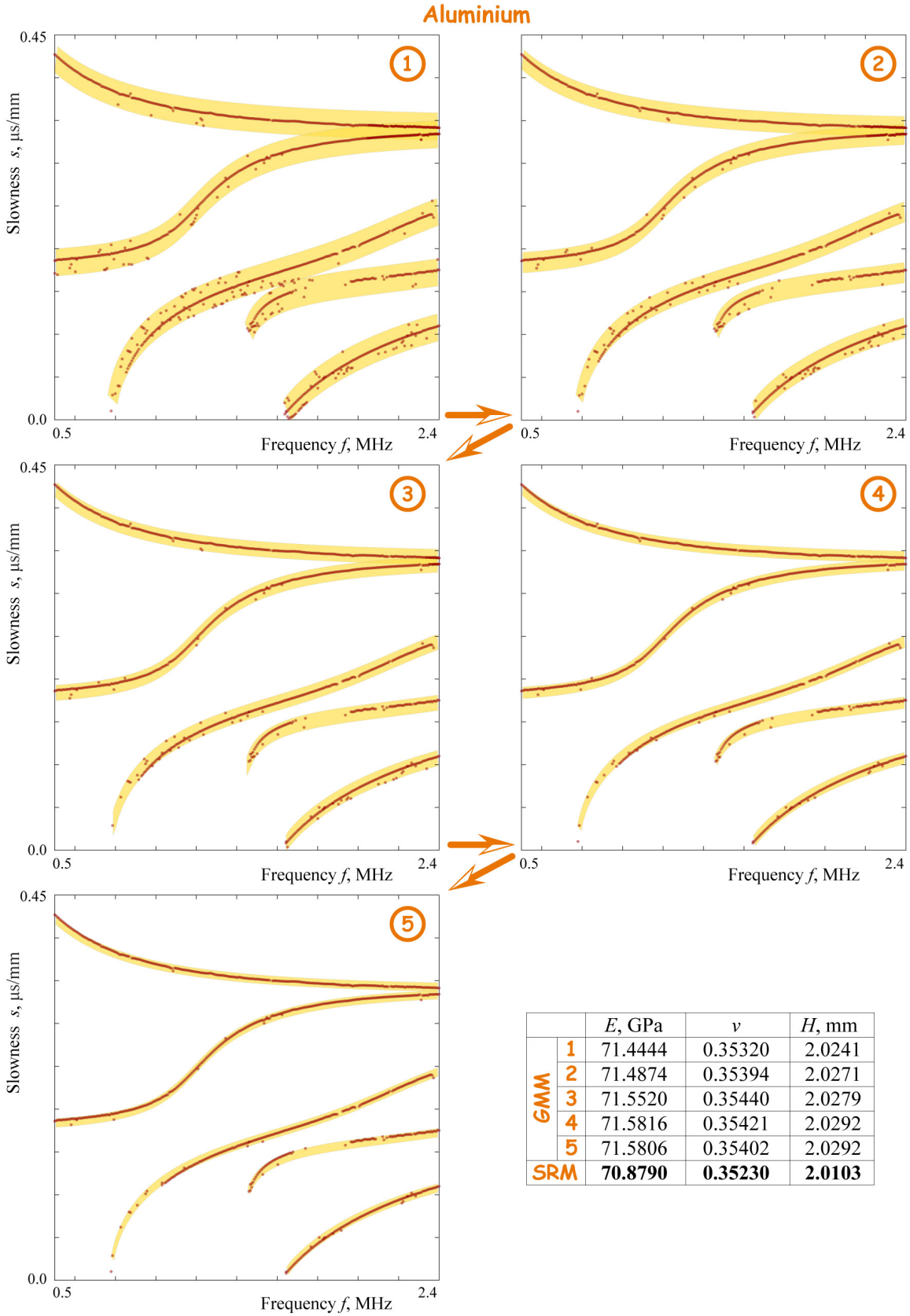

		E, GPa	ν	H, mm
GMM	1	71.4444	0.35320	2.0241
	2	71.4874	0.35394	2.0271
	3	71.5520	0.35440	2.0279
	4	71.5816	0.35421	2.0292
	5	71.5806	0.35402	2.0292
SRM		**70.8790**	**0.35230**	**2.0103**

Figure 4. Experimental slownesses $\breve{\boldsymbol{g}}^{(j)}$ filtered during the iterative process of *Step* 2 for aluminium plate with the mass density $\rho = 2660$ kg/m^3 and thickness $H = 2$ mm.

Preprints (www.preprints.org) | NOT PEER-REVIEWED | Posted: 5 May 2022 doi:10.20944/preprints202205.0050.v1

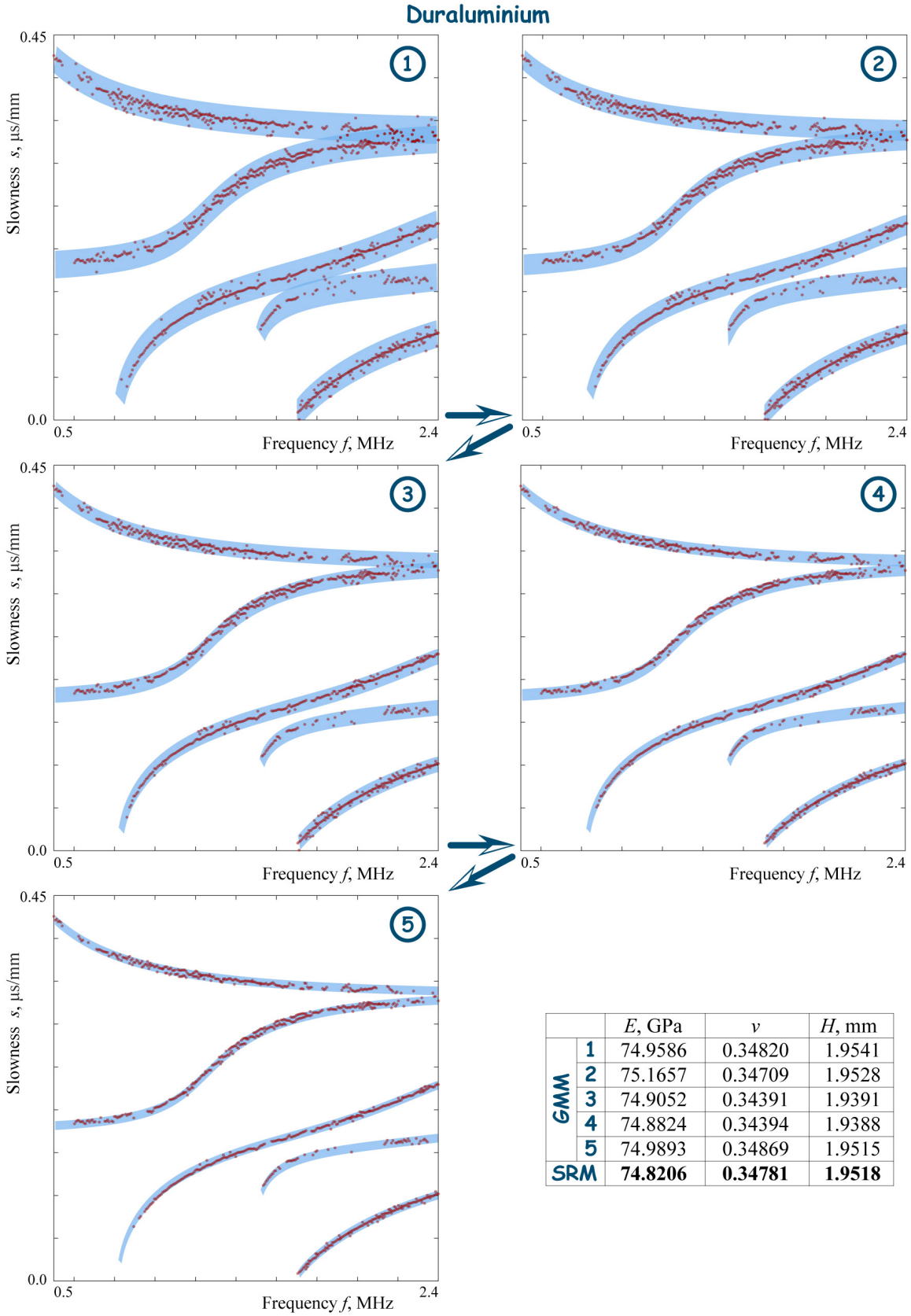

		E, GPa	ν	H, mm
GMM	1	74.9586	0.34820	1.9541
	2	75.1657	0.34709	1.9528
	3	74.9052	0.34391	1.9391
	4	74.8824	0.34394	1.9388
	5	74.9893	0.34869	1.9515
SRM		**74.8206**	**0.34781**	**1.9518**

Figure 5. Experimental $\breve{g}^{(j)}$ filtered during the iterative process of *Step* 2 for duraluminium plate with the mass density $\rho = 2721$ kg/m^3 and thickness $H = 1.9$ mm.

Preprints (www.preprints.org) | NOT PEER-REVIEWED | Posted: 5 May 2022 doi:10.20944/preprints202205.0050.v1

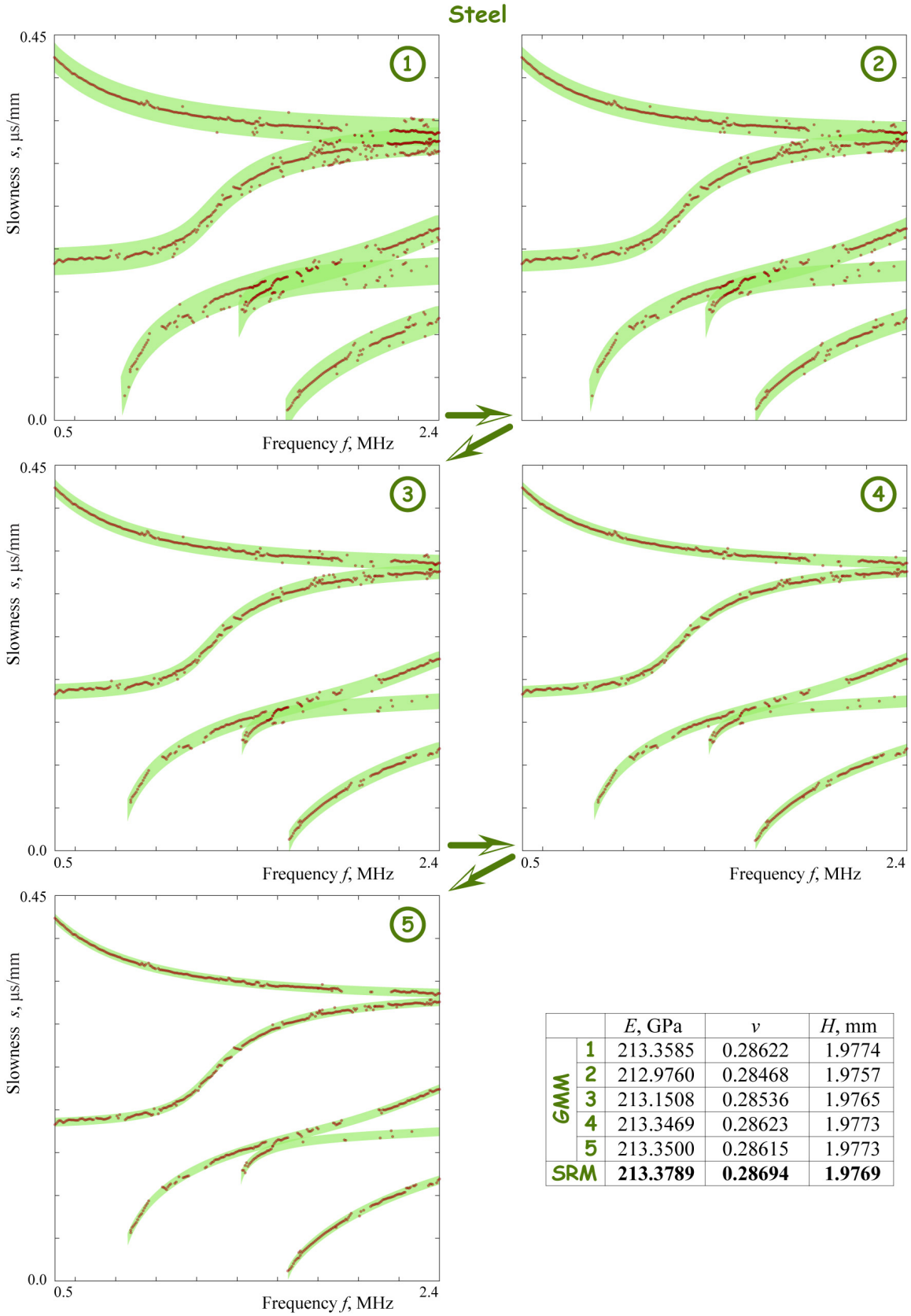

		E, GPa	ν	H, mm
GMM	1	213.3585	0.28622	1.9774
	2	212.9760	0.28468	1.9757
	3	213.1508	0.28536	1.9765
	4	213.3469	0.28623	1.9773
	5	213.3500	0.28615	1.9773
SRM		**213.3789**	**0.28694**	**1.9769**

Figure 6. Experimental slownesses $\breve{\boldsymbol{g}}^{(j)}$ filtered during the iterative process of *Step* 2 for steel plate with the mass density $\rho = 7843$ kg/m^3 and thickness $H = 1.975$ mm.

Preprints (www.preprints.org) | NOT PEER-REVIEWED | Posted: 5 May 2022 doi:10.20944/preprints202205.0050.v1

Out-of-plane velocities of propagating wave packages are measured at the surface of the specimen by PSV-500-V laser Doppler vibrometer (Polytec GmbH, Germany) [27]. The actuator has been driven by broadband 0.5 μs rectangular pulse tone burst voltage whose spectrum is non-zero for frequencies up to 3 MHz.

Figures 4–6 exhibit experimental slownesses $\check{\boldsymbol{g}}^{(j)}$ filtered during the iterative process of *Step* 2 for the three considered plates with the known mass density. The parameter values $\hat{\theta}_l^{(j)}$ for all the stages are shown in the table at the bottom of the figures. The solution of the optimization problems has been implemented in Python programming language, whereas the calculation of the Fourier transform of Green's matrix and the search root procedure has been implemented in the FORTRAN programming language to speed up the computations. One can see that though *Step* 2 already provides quite good estimations (at least for the thickness value, which might be easily obtained from the measurements), the SRM at *Step* 3 improves and statistically improves the results.

6. Discussions

The proposed numerical method of material properties identification allows for the processing of experimental line scans automatically with the minimal manual tuning of the parameters. Besides, its core functionality is not limited by the MPM as a tool for the evaluation of dispersion curves (i.e., the latter might be replaced by conventional wave-number frequency analysis [28] with further image processing to extract particular $(\check{s}_{nm}, f_n)$ pairs) and laser Doppler vibrometry as an experimental technique for UGW sensing (some other types of laser interferometers as well as broad-band air-coupled transducers could be adopted). Of course, the method might be improved by involving parallel computing of (7) for various initial values at *Step* 3, which is the most computationally expensive part. Another extension might be related to the data extraction using the MPM, where adaptive schemes are possible to reduce noise and smooth dispersion curves.

The employment of multi-objective optimization has allowed for the reduction of computational costs with the optimal accuracy of particular parameter identification. Efficient algorithms are available within the boundary integral equation method used in the present study [26,29,30] for the calculating the Fourier transform of Green's matrix and dispersion characteristics of multi-layered waveguides. Besides, The semi-analytical finite element method (SAFEM), which is one of the most popular techniques for computing the dispersion of guided waves, is also very effective for modelling guided waves propagation in laminates. Therefore, the improved unsupervised learning method presented here might be extended for inverse problem solutions involving multi-layered structures. The possible applications of the method include material properties identification in plates with thin coatings/interlayers anisotropic and laminates with a large number of sub-layers [31] as well as characterization of the severity of the degradation in laminates with degraded adhesive bondings [32].

Author Contributions: Conceptualization, M.V.G. and O.V.D.; methodology, M.V.G., O.V.D. and A.A.E.; software, M.A.A., O.V.D. and M.V.G; validation, I.A.B., O.V.D., M.A.A. and A.A.E.; formal analysis, O.V.D. and M.V.G.; investigation, O.V.D., M.V.G., Y.G. and A.A.E.; resources, A.A.E. and M.V.G.; data curation, I.A.B., O.V.D., M.A.A. and A.A.E.; writing—original draft preparation, M.V.G., O.V.D., A.A.E. and Y.G.; writing—review and editing, M.V.G., O.V.D., A.A.E. and Y.G.; visualization, M.V.G. and M.A.A.; project administration, M.V.G.; funding acquisition, M.V.G. and Y.G. All authors have read and agreed to the published version of the manuscript.

Funding: The research was carried out with the financial support of the Kuban Science Foundation in the framework of the project No. 20.1/118.

Institutional Review Board Statement: Not applicable

Informed Consent Statement: Not applicable

Data Availability Statement: Data sharing not applicable to this article as no datasets were generated or analyzed during the current study.

Acknowledgments: The authors express their deep gratitude to Prof. Rolf Lammering (Helmut Schmidt University, Hamburg, Germany) for the comprehensive support of the experimental investigations.

Conflicts of Interest: The authors declare no conflict of interest.

Abbreviations

The following abbreviations are used in this manuscript:

MPM	matrix pencil method
UGWs	ultrasonic guided waves
SRM	method based on the minimization of the slowness residuals
GMM	the method based on the calculation of the Fourier transform of Green's matrix

References

1. Cui, R.; Lanza di Scalea, F. Identification of Elastic Properties of Composites by Inversion of Ultrasonic Guided Wave Data. *Experimental mechanics* **2021**, *61*, 803–816. doi:10.1007/s11340-021-00700-1.
2. Tam, J.; Ong, Z.; Ismail, Z.; Ang, B.; Khoo, S. Identification of material properties of composite materials using nondestructive vibrational evaluation approaches: A review. *Mechanics of Advanced Materials and Structures* **2017**, *24*, 971–986. doi:10.1080/15376494.2016.1196798.
3. Lugovtsova, Y.; Bulling, J.; Boller, C.; Prager, J. Analysis of guided wave propagation in a multi-layered structure in view of structural health monitoring. *Applied Sciences* **2019**, *9*. doi:10.3390/app9214600.
4. Kralovec, C.; Schagerl, M. Review of Structural Health Monitoring Methods Regarding a Multi-Sensor Approach for Damage Assessment of Metal and Composite Structures. *Sensors* **2020**, *20*. doi:10.3390/s20030826.
5. Aabid, A.; Parveez, B.; Raheman, M.A.; Ibrahim, Y.E.; Anjum, A.; Hrairi, M.; Parveen, N.; Mohammed Zayan, J. A Review of Piezoelectric Material-Based Structural Control and Health Monitoring Techniques for Engineering Structures: Challenges and Opportunities. *Actuators* **2021**, *10*. doi:10.3390/act10050101.
6. Hughes, J.M.; Mohabuth, M.; Khanna, A.; Vidler, J.; Kotousov, A.; Ng, C.T. Damage detection with the fundamental mode of edge waves. *Structural Health Monitoring* **2021**, *20*, 74–83. doi:10.1177/1475921720920314.
7. Bai, L.; Le Bourdais, F.; Miorelli, R.; Calmon, P.; Velichko, A.; Drinkwater, B.W. Ultrasonic Defect Characterization Using the Scattering Matrix: A Performance Comparison Study of Bayesian Inversion and Machine Learning Schemas. *IEEE Transactions on Ultrasonics, Ferroelectrics, and Frequency Control* **2021**, *68*, 3143–3155. doi:10.1109/TUFFC.2021.3084798.
8. Ewald, V.; Sridaran Venkat, R.; Asokkumar, A.; Benedictus, R.; Boller, C.; Groves, R.M. Perception modelling by invariant representation of deep learning for automated structural diagnostic in aircraft maintenance: A study case using DeepSHM. *Mechanical Systems and Signal Processing* **2022**, *165*, 108153. doi:https://doi.org/10.1016/j.ymssp.2021.108153.
9. Cui, R.; Lanza di Scalea, F. On the identification of the elastic properties of composites by ultrasonic guided waves and optimization algorithm. *Composite Structures* **2019**, *223*, 110969. doi:https://doi.org/10.1016/j.compstruct.2019.110969.
10. Araque, L.; Wang, L.; Mal, A.; Schaal, C. Advanced fuzzy arithmetic for material characterization of composites using guided ultrasonic waves. *Mechanical Systems and Signal Processing* **2022**, *171*, 108856. doi:https://doi.org/10.1016/j.ymssp.2022.108856.
11. Chen, Q.; Xu, K.; Ta, D. High-resolution Lamb waves dispersion curves estimation and elastic property inversion. *Ultrasonics* **2021**, *115*, 106427. doi:https://doi.org/10.1016/j.ultras.2021.106427.
12. Chang, C.; Yuan, F. Dispersion curve extraction of Lamb waves in metallic plates by matrix pencil method. 2017, Vol. 10168. doi:10.1117/12.2259790.
13. Pogorelyuk, L.; Rowley, C.W. Clustering of Series via Dynamic Mode Decomposition and the Matrix Pencil Method. *arXiv: Numerical Analysis* **2018**.
14. Okumura, S.; Nguyen, V.H.; Taki, H.; Haïat, G.; Naili, S.; Sato, T. Rapid High-Resolution Wavenumber Extraction from Ultrasonic Guided Waves Using Adaptive Array Signal Processing. *Applied Sciences* **2018**, *8*. doi:10.3390/app8040652.
15. Liu, Z.; Xu, K.; Li, D.; Ta, D.; Wang, W. Automatic mode extraction of ultrasonic guided waves using synchrosqueezed wavelet transform. *Ultrasonics* **2019**, *99*, 105948. doi:https://doi.org/10.1016/j.ultras.2019.105948.
16. Xu, K.; Ta, D.; Moilanen, P.; Wang, W. Mode separation of Lamb waves based on dispersion compensation method. *The Journal of the Acoustical Society of America* **2012**, *131*, 2714–2722. doi:10.1121/1.3685482.
17. Gu, M.; Li, Y.; Tran, T.N.; Song, X.; Shi, Q.; Xu, K.; Ta, D. Spectrogram decomposition of ultrasonic guided waves for cortical thickness assessment using basis learning. *Ultrasonics* **2022**, *120*, 106665. doi:https://doi.org/10.1016/j.ultras.2021.106665.
18. Ren, L.; Gao, F.; Wu, Y.; Williamson, P.; Wang, W.; McMechan, G.A., Automatic picking of multi-mode dispersion curves using CNN-based machine learning. In *SEG Technical Program Expanded Abstracts 2020*; 2020; pp. 1551–1555. doi:10.1190/segam2020-3427827.1.
19. Zhang, J.; He, Q.; Xiao, Y.; Zheng, H.; Wang, C.; Luo, J. Self-Supervised Learning of a Deep Neural Network for Ultrafast Ultrasound Imaging as an Inverse Problem. 2020 IEEE International Ultrasonics Symposium (IUS), 2020, pp. 1–4. doi:10.1109/IUS46767.2020.9251533.

20. Rautela, M.; Gopalakrishnan, S.; Gopalakrishnan, K.; Deng, Y. Ultrasonic Guided Waves Based Identification of Elastic Properties Using 1D-Convolutional Neural Networks. 2020 IEEE International Conference on Prognostics and Health Management (ICPHM), 2020, pp. 1–7. doi:10.1109/ICPHM49022.2020.9187057.
21. Gopalakrishnan, K.; Rautela, M.; Deng, Y. Deep Learning Based Identification of Elastic Properties Using Ultrasonic Guided Waves. European Workshop on Structural Health Monitoring; Rizzo, P.; Milazzo, A., Eds.; Springer International Publishing: Cham, 2021; pp. 77–90.
22. Li, Y.; Xu, K.; Li, Y.; Xu, F.; Ta, D.; Wang, W. Deep Learning Analysis of Ultrasonic Guided Waves for Cortical Bone Characterization. *IEEE Transactions on Ultrasonics, Ferroelectrics, and Frequency Control* **2021**, *68*, 935–951. doi:10.1109/TUFFC.2020.3025546.
23. Tam, J.H. Identification of elastic properties utilizing non-destructive vibrational evaluation methods with emphasis on definition of objective functions: a review. *Structural and Multidisciplinary Optimization* **2020**, *61*, 1677–1710. doi:10.1007/s00158-019-02433-1.
24. Golub, M.V.; Doroshenko, O.V.; Arsenov, M.; Bareiko, I.; Eremin, A.A. Identification of material properties of elastic plate using guided waves based on the matrix pencil method and laser Doppler vibrometry. *Preprints* **2022**. doi:10.20944/preprints202204.0161.v1.
25. Nozato, H.; Kokuyama, W.; Shimoda, T.; Inaba, H. Calibration of laser Doppler vibrometer and laser interferometers in high-frequency regions using electro-optical modulator. *Precision Engineering* **2021**, *70*, 135–144. doi:https://doi.org/10.1016/j.precisioneng.2021.
26. Glushkov, E.V.; Glushkova, N.V. On the efficient implementation of the integral equation method in elastodynamics. *Journal of Computational Acoustics* **2001**, *9(3)*, 889–898. doi:10.1142/S0218396X01001169.
27. Neumann, M.N.; Hennings, B.; Lammering, R. Identification and Avoidance of Systematic Measurement Errors in Lamb Wave Observation With One-Dimensional Scanning Laser Vibrometry. *Strain* **2013**, *49*, 95–101. doi:https://doi.org/10.1111/str.12015.
28. Alleyne, D.N.; Cawley, P. A two-dimensional Fourier transform method for the measurement of propagating multimode signals. *The Journal of the Acoustical Society of America* **1991**, *89*, 1159–1168. doi:10.1121/1.400530.
29. Glushkov, E.; Glushkova, N.; Eremin, A. Forced wave propagation and energy distribution in anisotropic laminate composites. *Journal of the Acoustical Society of America* **2011**, *129*, 2923–2934. doi:10.1121/1.3559699.
30. Fomenko, S.I.; Golub, M.V.; Doroshenko, O.V.; Wang, Y.; Zhang, C. An advanced boundary integral equation method for wave propagation analysis in a layered piezoelectric phononic crystal with a crack or an electrode. *Journal of Computational Physics* **2021**, *447*. doi:10.1016/j.jcp.2021.110669.
31. Wilde, M.V.; Golub, M.V.; Eremin, A.A. Elastodynamic behaviour of laminate structures with soft thin interlayers: theory and experiment. *Materials* **2022**, *15*, 1307. doi:doi.org/10.3390/ma15041307.
32. Golub, M.V.; Doroshenko, O.V.; Wilde, M.V.; Eremin, A.A. Experimental validation of the applicability of effective spring boundary conditions for modelling damaged interfaces in laminate structures. *Composite Structures* **2021**, *273*, 114141. doi:10.1016/j.compstruct.2021.114141.